CrystEngComm

Accepted Manuscript

ROYAL SOCIETY OF CHEMISTRY

www.rsc.org/crystengcomm

Transition metal coordination complexes of chrysazin†

Patrick J. Beldon,[a] Sebastian Henke,[ab] Bartomeu Monserrat,[c] Satoshi Tominaka,[ad] Norbert Stock,[e] and Anthony K. Cheetham*[a]

Received Xth XXXXXXXXXX 20XX, Accepted Xth XXXXXXXXX 20XX
First published on the web Xth XXXXXXXXXX 200X
DOI: 10.1039/b000000x

Eleven novel coordination compounds, composed of chrysazin (1,8-dihydroxyanthraquinone) and different first-row transition metals (Fe, Co, Ni, Cu), were synthesised and the structures determined by single-crystal X-ray diffraction. The synthetic trends were investigated using high-throughput synthesis under systematic variation of concentration and reagent stoichiometry: for complexes containing Co, Ni or Cu crystallisation was improved by low ligand:metal ratios, while the effect of concentration depended on the metal used. The compounds crystallise as discrete clusters, apart from two, which contain long Cu-O bonds which may allow the two compounds to be considered one-dimensional coordination polymers. One of these compounds shows a distance between aryl rings of less than 3.26 Å, which is shorter than that in graphite, suggesting applications as an organic-inorganic semiconductor. The compound was found to be insulating by single-crystal and powder AC-impedance measurements, and this result is discussed with reference to the electronic structure calculated using density-functional theory.

Introduction

Anthraquinones are optically- and redox-active molecules, thanks to their large π-systems.[1] The presence of carbonyl groups in anthraquinones increases the electron affinity of the molecules compared to their acene counterparts, making anthraquinones electron acceptors. This combination of properties makes anthraquinones attractive for use in organic electronics, where electron accepting (n-type) conductors are much more scarce than electron donating (p-type) conductors.[2–4] The application of anthraquinones in organic electronics is limited by the low electron mobilities typically seen in anthraquinone crystals/films.[2] Attempts in crystal engineering to improve mobilities in organic electronics typically aim for closer π-stacking between molecules.[5–8] Furman et al showed that the luminescence of anthraquinone ligands can be modulated by incorporation into an organic-inorganic framework.[9] In that case the room temperature luminescence was quenched due to the increased flexibility of the system; however, this fact suggests that constraining anthraquinones into a more rigid framework may stabilise the excited states and result in electrical conduction. Herein, we report crystal engineering of an anthraquinone derivative, chrysazin (also known as 1,8-dihydroxyanthraquinone, Fig. 1), by forming coordination complexes with transition metals.

Coordination complexes of anthraquinones have applications as dyes and show interesting biological activity.[10] The presence of two phenolic hydrogens means that chrysazin is acidic and there is the potential for chelation between the phenol and quinone oxygens (between positions 1 and 9, and between positions 8 and 9). Chrysazin has been incorporated into a crown-ether-type molecule which is then able to selectively detect metal ions, using switchable luminescence from the chrysazin moiety.[11,12] Two Ag(I) coordination compounds were reported using chrysazin derivatives, modified by covalently adding chelating thioether groups via the phenolic oxygens (positions 1 and 8, see Fig. 1).[13] The optical properties of presumed metal-chrysazinate complexes have been studied in solution with a wide range of metals, including transition metals, lanthanides and group 13 metals.[14] Despite this, to our knowledge, no structures of chrysazinate coordination complexes have been determined.

To gain a greater understanding of anthraquinone-based coordination complexes and polymers, we undertook structural analysis of chrysazin coordination complexes by single-crystal X-ray diffraction. Furthermore, in order to obtain

† Electronic Supplementary Information (ESI) available: [Full experimental details, PXRD data, IR spectra, DFT results at different pressures]. See DOI: 10.1039/b000000x/. CCDC 1044027-1044037 contains the supplementary crystallographic data for this paper. These data can be obtained free of charge from The Cambridge Crystallographic Data Centre via www.ccdc.cam.ac.uk/data_request/cif.

[a] *Department of Materials Science & Metallurgy, University of Cambridge, 27 Charles Babbage Road, Cambridge, CB3 0FS, UK. E-mail: akc30@cam.ac.uk*
[b] *Lehrstuhl für Anorganische Chemie II, Ruhr-Universität Bochum, 44780 Bochum, Germany.*
[c] *Department of Physics, University of Cambridge, Cavendish Laboratory, JJ Thomson Avenue, Cambridge, CB3 0HE, UK.*
[d] *International Center for Materials Nanoarchitectonics (WPI-MANA), National Institute for Materials Science (NIMS), Ibaraki 305-0044, Japan.*
[e] *Institut für Anorganische Chemie, Christian-Albrechts-Universität, Max-Eyth Straße 2, D 24118 Kiel, Germany.*

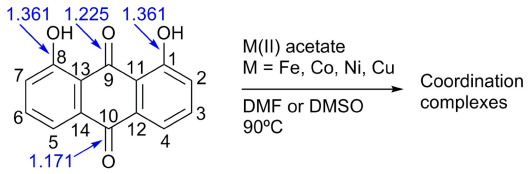

Fig. 1 Overall synthetic scheme, with the labelling convention for anthraquinone derivatives. The oxygen atoms will be referred to by the number of the carbon atom to which they are bonded. The carbon-oxygen bond lengths (Å, at 295 K) have been labelled from Cambridge Structural Database entry DHANQU07.[15]

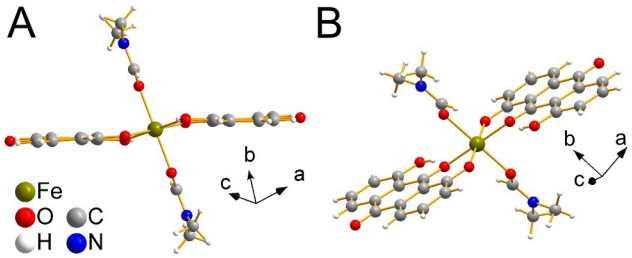

Fig. 2 Two different views of the structure of **FeChrys-1**, [Fe(HChrysazinate)$_2$DMF$_2$].

insight on the effect of π-π overlap between adjacent anthraquinone molecules, we systematically synthesized a variety of chrysazin coordination complexes using conventional and high-throughput solvothermal synthesis methods.

Methods

Full experimental details are given in the electronic supplementary information (ESI).† Standard reactions were carried out at 90 °C in 20 ml glass vials, using 4-10 ml dimethylformamide (DMF) or dimethylsulfoxide (DMSO) as a solvent and a ligand:metal molar ratio of 1:2 (except for **FeChrys-1**, **FeChrys-2** and **NiNOChrys-1** which used a 1:1 molar ratio). **CoChrys-1**, **NiChrys-1**, **CuChrys-1**, **CuChrys-2** and **CuChrys-4** all formed in the reaction of chrysazin with the respective metal(II) acetate. **FeChrys-1** and **FeChrys-2** were found in the reaction between Fe(AcO)$_2$ and chrysazin in deaerated DMF. This reaction proved difficult to reproduce: **FeChrys-2** formed in a reaction that was a repeat of the reaction to form **FeChrys-1** and the difference in oxidation state between these complexes suggests that dissolved oxygen may have a role. The inclusion of pyridine in the reaction between Co(AcO)$_2$·4H$_2$O and chysazin gave **CoChrys-2**. The reaction between Co(OH)$_2$ and chrysazin in deaerated DMF gave **CoChrys-3** which we could characterise using SCXRD; however, we were unable to reproducibly make this product. Using dimethylsulfoxide (DMSO) instead of DMF in the copper system gave **CuChrys-3**. The reaction of 4,5-dinitrochrysazin with Ni(AcO)$_2$ in a 1:1 molar ratio gave **NiNOChrys-1**. Exploratory reactions were tried using the same metal salts and ligands at room temperature; however, only starting materials were recovered from these attempts and so it appears that heating is necessary to drive the reactions.

High-throughput reactions were carried out on a 2-20mg scale and ran for 18 hours in 1 ml DMF in 2 ml teflon containers contained in a high-throughput autoclave, capable of holding 24 teflon containers.[16,17] We carried out screening reactions between chrysazin and Co(AcO)$_2$·4H$_2$O, Ni(AcO)$_2$·4H$_2$O and Cu(AcO)$_2$·4H$_2$O. Mn(AcO)$_2$·4H$_2$O and Fe(AcO)$_2$ were also screened, though no crystalline products were found for these metals. The conditions screened were metal:ligand ratio and concentration of reactants (see Tables 2 to 4).

Results and discussion

Crystal structures

Eleven transition metal-chrysazinate complexes have been synthesized and their structures characterized via single crystal X-ray diffraction; in the paragraphs below, we describe the structures in detail. We denote the neutral ligand as Chrysazin, the singly-deporotonated ligand as HChrysazinate and the doubly-deprotonated ligand as Chrysazinate. The crystallographic data are summarised in Tables S3 to S5.

FeChrys-1, [Fe(HChrysazinate)$_2$DMF$_2$], crystallises in the monoclinic space group $P2_1/n$ giving black, needle-shaped crystals. **FeChrys-1** contains a complex with one octahedral Fe^{2+} ion, chelated by two singly-protonated chrysazinate anions, with coordinated DMF molecules in the axial positions (Fig. 2). The asymmetric unit contains half of this complex, with the Fe^{2+} ion on an inversion centre. This is the only complex structurally characterised so far in which one of the hydroxyl groups of chrysazin remains protonated. There is one reasonably short π-π stacking distance in the structure (3.423 Å plane-plane, calculated from mean-planes with all carbon atoms of one HChrysazinate moiety using the program Olex2[18]); however, there is no extended network of π-stacking.

FeChrys-2, [Fe$_2$(Chrysazinate)$_3$]·DMF·$\frac{1}{2}$H$_2$O, forms black, lathe crystals and crystallises in the triclinic space group $P\bar{1}$. The molecular complex in **FeChrys-2** is made up of two Fe^{3+} ions coordinated to three chrysazinate dianions. The metal ions adopt highly distorted octahedral geometries, and the octahedra are face-sharing. The chrysazinate ligands coordinate such that the complex has a 3-armed paddlewheel structure (Fig. 3A & B). The asymmetric unit of **FeChrys-2**

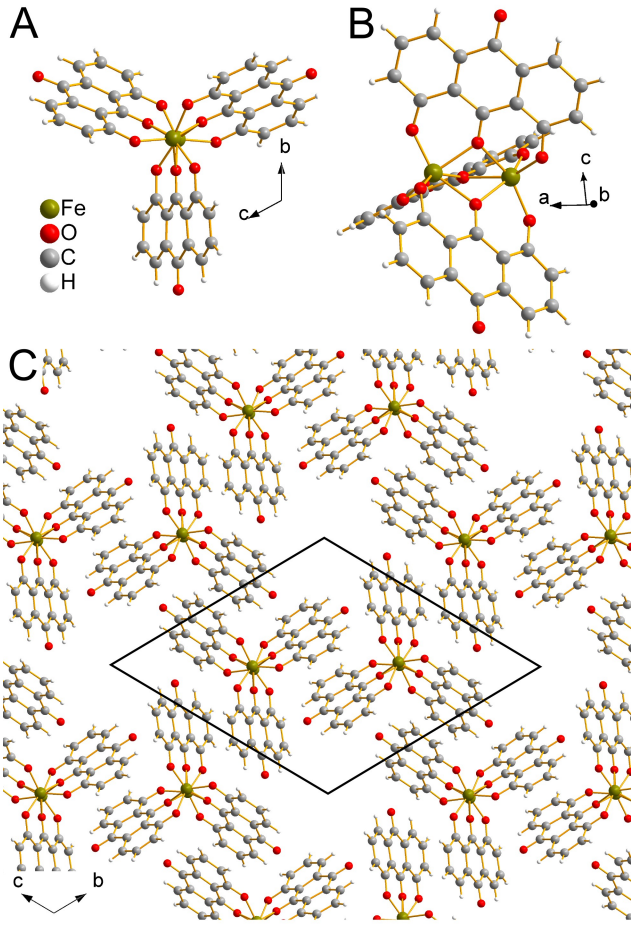

Fig. 3 Structure of **FeChrys-2**, $[Fe_2(Chrysazinate)_3]\cdot DMF\cdot\frac{1}{2}H_2O$. (A) & (B) Two different views of the asymmetric unit/molecular complex in **FeChrys-2**. (C) View down the *a* axis, highlighting channels formed between the iron paddlewheel units. The non-coordinated DMF and H_2O sit in these channels but have been omitted from the figure for clarity.

contains one of these complexes, plus one molecule of non-coordinated DMF and a half-occupied molecule of non-coordinated H_2O. The paddlewheel complexes pack into an hexagonal arrangement (Fig. 3C), with channels running down the *a* direction, and the non-coordinated solvent sits in these channels. Each chrysazinate ligand is slip-stacked face-to-face with a chrysazinate ligand in a neighbouring complex with plane-plane distances of 3.379(3) to 3.447(3) Å and centroid-centroid distances of 4.856(2) to 4.996(2) Å. While the complex is chiral, the crystal is racemic, having both enantiomers within the unit cell related to each other by the inversion centre of the space group.

CoChrys-1, $[Co_{12}(Chrysazinate)_6(AcO)_{12}DMF_6]\cdot 6(DMF)$, crystallises as black, block-shaped crystals in the trigonal space group $R\bar{3}$ and contains molecular complexes with crystallographically imposed $\bar{3}$ symmetry, based on a ring of 12 Co^{2+} ions, each coordinated in an approximately octahedral geometry (Fig. 4A & B). The Co-O octahedra are arranged in an edge-sharing fashion to form the ring of 12 cobalt ions. The asymmetric unit contains two cobalt ions coordinated to one chrysazinate dianion, two acetate anions and one coordinated DMF molecule. Each chrysazinate coordinates to four metal ions, with the 1, 8 and 9 position oxygens forming μ_2-oxo bridges between the four metal centres. In each Co_{12} cluster, three chrysazinate molecules coordinate from above the plane of the ring, and three from below, forming a pocket on each side. Such an arrangement is reminiscent of molecules such as cyclodextrins or cucurbiturils that are used in supramolecular chemistry for molecular recognition and the self-assembly of supramolecular entities.[19,20] The two pockets are separated from each other by coordinated acetate anions which sit roughly in the plane of the ring.

The ring-shaped Co_{12} clusters stack into columns with the rings lining up with one another down the *c* axis. These columns pack into a hexagonal arrangement with the columns being displaced along the *c* axis by $c/3$ or $2c/3$, with respect to their adjacent columns (Fig. 4C). In contrast to the iron complexes discussed above, there is no π-π stacking between chrysazinate ligands of adjacent complexes. The pockets of neighbouring molecules face each other, forming a large pore. This pore is filled with non-coordinated DMF molecules which are highly disordered. Unfortunately, it was impossible to accurately model and refine the positions of the DMF molecules and, as a result, the residual electron density assigned to the non-coordinated DMF guests was subtracted from the data using the SQUEEZE algorithm in the PLATON program package.[21,22] Three symmetry related voids of about 864 to 867 $Å^3$ have been found per unit cell, each containing about 200 electrons. A DMF molecule contains 40 electrons, suggesting the presence of 5 DMF molecules per void and an approximate composition of $[Co_{12}(Chrysazinate)_6(AcO)_{12}DMF_6]\cdot 5(DMF)$. By thermal and elemental analysis (see ESI) we found that the pores contain 6 DMF molecules per molecule of $[Co_{12}(Chrysazinate)_6(AcO)_{12}DMF_6]$, in reasonable agreement with the crystallographic estimation. The IR spectrum is consistent with the presence of DMF, but shows no trace of water or acetic acid so it appears that DMF is the only non-coordinated guest present in significant quantities (Fig. S3).

CoChrys-2, $[Co_3(Chrysazinate)_2(AcO)_2DMF_3Pyridine]$, forms black, block-shaped crystals that crystallise in the triclinic space group $P\bar{1}$. The asymmetric unit of **CoChrys-2** contains three Co^{2+} ions, two chrysazinate dianions, two acetate anions, three coordinated DMF molecules and one coordinated molecule of pyridine. Each Co^{2+} adopts a distorted

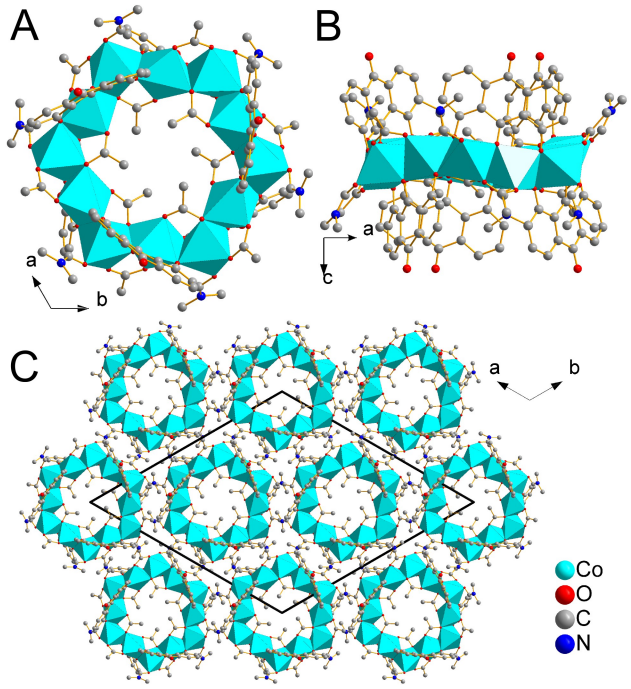

Fig. 4 Structure of **CoChrys-1**, $[Co_{12}(Chrysazinate)_6(AcO)_{12}DMF_6]\cdot 6(DMF)$, which is isomorphous with **NiChrys-1** $[Ni_{12}(Chrysazinate)_6(AcO)_{12}DMF_6]\cdot 6(DMF)$. Disordered DMF guests have not been included in the structural model and H atoms have been omitted for clarity. (A) View down the *c* axis of the $[Co_{12}(Chrysazinate)_6(AcO)_{12}DMF_6]$ ring. (B) View down the *a* axis of the $[Co_{12}(Chrysazinate)_6(AcO)_{12}DMF_6]$ ring. (C) Packing of the structure, viewed down the *c* axis.

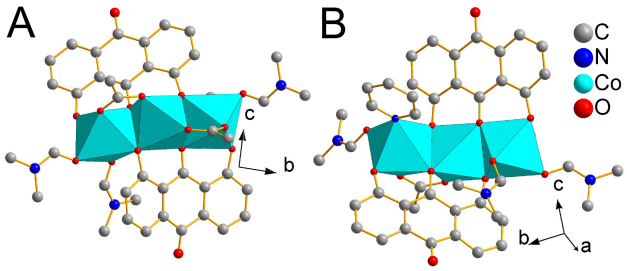

Fig. 5 Two different views of the structure of **CoChrys-2**, $[Co_3(Chrysazinate)_2(AcO)_2DMF_3Pyridine]$. H has been omitted for clarity.

octahedral geometry (Fig. 5) and the octahedra are edge-sharing with adjacent octahedra.

CoChrys-3, $2[Co_4(Chrysazinate)_4DMF_4]\cdot 2.35(DMF)\cdot\frac{1}{2}H_2O$, crystallises as red, needle-shaped crystals in the space group $P\bar{1}$. The complex contains four Co^{2+} ions, each in a distorted octahedral environment with an oxygen atom at each vertex, either from a chrysazinate dianion or a DMF molecule. The octahedra are arranged in a square in an edge-sharing fashion. Chrysazinate dianions are coordinated perpendicular to the plane of Co ions, two above and two below the plane. Four DMF molecules are coordinated axially to this plane. In each asymmetric unit there are two of these complexes. Two of the four chrysazinate ligands in each complex are disordered and we accounted for this using a model split over two sites. The structure also contains uncoordinated solvent and we were able to refine one fully-occupied DMF molecule, two half-occupied DMF molecules and a half-occupied water molecule; however there was residual electron density which was subtracted from the experimental data using the SQUEEZE algorithm in PLATON, which gave a void of 328 $Å^3$ and 28 electrons. These 28 electrons would correspond to additional 0.7 DMF molecules per unit cell, or 0.35 per formula unit (see Crystallographic Information File for details).[21,22]

NiChrys-1, $[Ni_{12}(Chrysazinate)_6(AcO)_{12}DMF_6]\cdot 6(DMF)$, crystallises as black, block-shaped crystals in the trigonal space group $R\bar{3}$. **NiChrys-1** is isostructural and isomorphous with **CoChrys-1**, with unit cell parameters that agree to within 0.02 Å, again giving complexes of rings of 12 nickel atoms with crystallographically imposed $\bar{3}$ symmetry. Despite the overall similarity, the metal polyhedra are larger and more distorted in **CoChrys-1** than in **NiChrys-1** (Table 1), as expected given the respective ionic radii and the Jahn-Teller effect arising from the degenerate electronic configuration of octahedrally coordinated cobalt d^7.[23]

NiChrys-2, $[Ni_6(Chrysazinate)_4(AcO)_4DMF_4]\cdot 4(DMF)$, crystallises as red, block-shaped crystals in the triclinic space

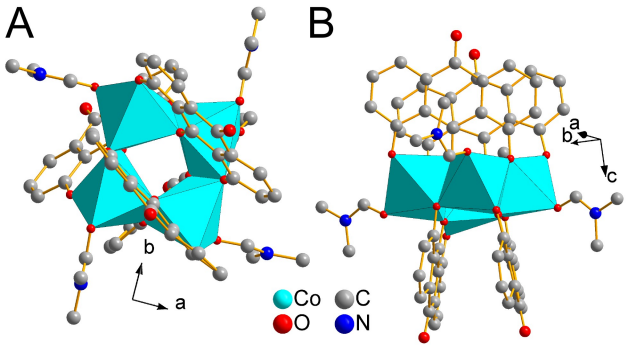

Fig. 6 Two different views of the molecular structure of **CoChrys-3**, $2[Co_4(Chrysazinate)_4DMF_4]\cdot 2.35(DMF)\cdot\frac{1}{2}H_2O$. H atoms have been omitted for clarity. The asymmetric unit contains two crystallographically independent clusters (only one is shown due to the close similarity of the structures). Two of the chrysazinate ligands in each cluster are disordered, and this has been hidden from the diagram for clarity; full details are included in the CIF.

	NiChrys-1		**CoChrys-1**	
	Ni1	Ni2	Co1	Co2
Volume of M-O octahedra (Å^3)	11.23	11.16	11.73	11.64
Average deviation of O-M-O bond angles from perpendicular (°)	5.33	6.39	6.17	7.40

Table 1 Geometric parameters for the metal-oxygen (M-O) octahedra in **NiChrys-1** and **CoChrys-1**. Standard deviations are below the precision given.

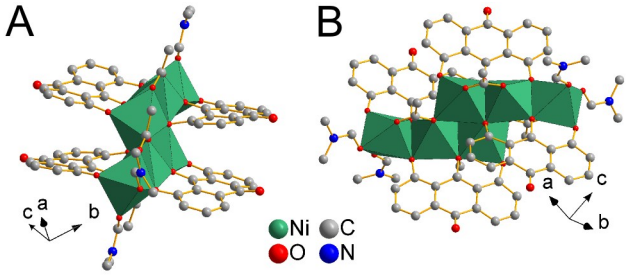

Fig. 7 Two different views of the structure of **NiChrys-2**, $[Ni_6(Chrysazinate)_4(AcO)_4DMF_4]\cdot 4(DMF)$. Non-coordinated DMF molecules and H atoms have been hidden from the structure for clarity.

group $P\bar{1}$. The asymmetric unit of **NiChrys-2** contains three Ni^{2+} ions coordinated to two chrysazinate dianions, two acetate anions and two coordinated DMF molecules. In addition, there are also two molecules of uncoordinated DMF. Within the asymmetric unit, the three nickel ions are octahedrally coordinated to oxygen atoms and held in a line (Ni1, Ni2, Ni3). The nickel coordination octahedra are edge sharing: Ni1 with Ni2, Ni2 with Ni3. These trimers are linked to a crystallograhically equivalent trimer to form a hexamer and the coordination polyhedra are linked between these trimers in an edge sharing fashion: Ni1 with the opposing Ni1 and Ni2; Ni2 also links to the opposing Ni2; Ni3 does not link to the other trimer (Fig. 7). In the Ni_6 cluster, two chrysazinate molecules have a position 1 oxygen with triply bridging (μ^3) coordination to Ni^{2+}.

CuChrys-1, $[Cu_2(Chrysazinate)_2]$ forms black plate-like crystals and crystallises in the monoclinic space group $P2_1/c$. The asymmetric unit of **CuChrys-1** contains two chrysazinate dianions coordinated to two Cu^{2+}cations (Fig. 8A). The copper centres adopt a square planar geometry, with two oxygens of each chrysazinate coordinating to each copper ion in a bidentate fashion. The two chrysazinate molecules are coplanar; the RMS deviation of carbon atoms from a plane containing the carbon atoms of the two chrysazinate molecules is only 0.067 Å. These planar units form dimers, with the quinone oxygens (O10) coordinating at the axial position of one of the copper atoms on a second planar unit (Fig. 8B). These Cu-O bonds are 2.769(2) Å long (much longer than the sum of the Shannon radii[24,25] for Cu^{2+} and O of 2.0 Å) and pull the oxygens out of planarity with the rest of the molecule. There is an even longer bond of 3.126(3) Å between the O10 of the other chrysazinate and the free copper on the adjacent dimer. This again, slightly pulls the oxygen out of the plane of the molecule, but the effect is less pronounced. Taking these bonds into account, the metal geometry is square-based pyramidal (common for Jahn-Teller distorted d^9 Cu^{2+}) and the compound could be considered a 1D-coordination poly-

mer; however, the length of these bonds implies that they are weak. Hence, we regard **CuChrys-1** as a 0D-molecular structure. The dimers pack into a "brick-wall" architecture, forming a 2D π-bonded sheet (Fig. 8C). The π-stacking distances within these layers are remarkably short, giving plane-plane distances of 3.2593(14) Å and 3.1342(12) Å (based on mean-planes calculated using all of the carbon atoms in an asymmetric unit). For reference, graphite has a plane-plane distance of 3.354 Å.[26] Such short π-stacking distances are more common in coordination compounds than in purely organic crystals and a number of compounds with short stacking distances have been reported.[27–29] In the case of Cu(TCNQ) (TCNQ = 7,7,8,8-tetracyanoquinodimethane), the short π-stacking distance of 3.24 Å provides a pathway for electrical conductivity.[30] For the distance of 3.2593 Å, the π-system of chrysazinate faces another chrysazinate π-system, giving good π-overlap; for the distance of 3.1342 Å, the π-system of chrysazinate faces the Cu-O section of the complex, so there is no π-stacking between the carbon rings. These π-stacked layers are then misaligned with the next layer by a dihedral angle of 68.37° (Fig. 8D).

CuChrys-2, $[Cu_2(Chrysazinate)_2]\cdot 0.44DMF$ forms black, needle-like crystals in the space group $R\bar{3}$. A phase pure sample of this product could not be obtained and was found together with **CuChrys-1** (see the section Synthetic Trends for further details), suggesting that it is an intermediate product of the reaction. The asymmetric unit contains one Cu^{2+} ion and one chrysazinate dianion. The Cu^{2+} ions are coordinated within the $[Cu_2(Chrysazinate)_2]$ units in a similar fashion to **CuChrys-1**; however, the chrysazinate molecules are tilted out of planarity with each other. The $[Cu_2(Chrysazinate)_2]$ units stack into 1D chains, with a long (2.556(12) Å) bond between O8 of chrysazinate, to one of the Cu^{2+} ions on an adjacent $[Cu_2(Chrysazinate)_2]$ unit. The chrysazinate π-systems stack in a face-to-face fashion with a plane-plane distance of 3.283(4) Å, (calculated from the mean plane of the carbon atoms on one chrysazinate unit). The 1D chains pack in a Kagome lattice arrangement, leaving hexagonal 1D channels which make up 16.7 % of the unit cell volume (calculated by SQUEEZE/PLATON). These voids are full of non-coordinated solvent; unfortunately due to disorder, it was not possible to model this solvent so the residual electron density (53 electrons per void) was subtracted from the raw data using the SQUEEZE algorithm of the PLATON program package.[21,22]

CuChrys-3, $[Cu_2(Chrysazinate)_2DMSO_2]$ crystallises in the space group $Pca2_1$ and forms black block crystals. The Cu^{2+} ions and chrysazinate dianions coordinate in a dimeric motif similar to **CuChrys-1** and **CuChrys-2**, with one DMSO molecule coordinating to each Cu in an apical site to give a square-pyramidal geometry (Fig10). The DMSO molecules

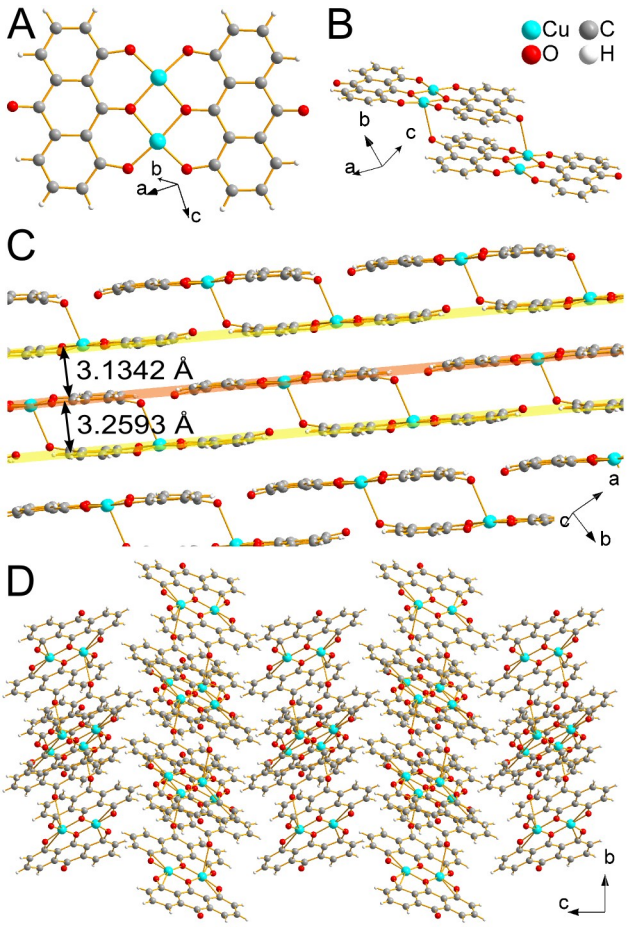

Fig. 8 Structure of **CuChrys-1**, $[Cu_2(Chrysazinate)_2]$. (A) Asymmetric unit, showing a planar $[Cu_2(Chrysazinate)_2]$ monomeric unit. (B) These planar units form dimers with bonds between the quinone oxygen and one copper on an adjacent monomer unit. (C) These monomers are arranged in a "brick-wall" architecture with short π-π distances. (D) The chrysazinate planes in the brick-wall layers are aligned at a dihedral angle of 68.37° to the chrysazinate planes in adjacent brick-wall layers.

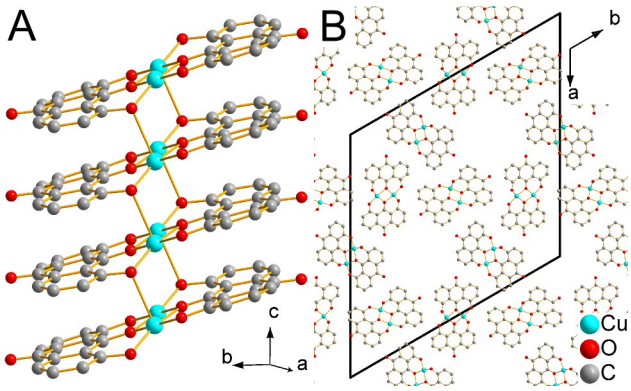

Fig. 9 Structure of $[Cu_2(Chrysazinate)_2]\cdot 0.44DMF$, **CuChrys-2**. (A) View of the 1D chains. (B) Unit cell showing the packing of the chains. The pores contain disordered DMF which has not been included in the structural model.

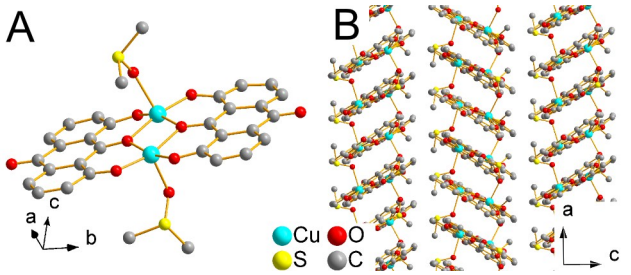

Fig. 10 Structure of $[Cu_2(Chrysazinate)_2DMSO_2]$, **CuChrys-3**. (A) View of the complex. (B) Packing of the complexes into layers. The S atoms of the DMSO ligands are disordered over two positions. Only the main component is shown here for clarity. H atoms have been omitted.

are disordered which was accounted for by a split model. The complexes pack into columns along the *a* axis, which interdigitate slightly along the *b* axis; however, this does not lead to close π-π stacks and the centroid-centroid distance between chrysazin moieties is only 4.14 Å.

NiNOChrys-1, $[Ni_2(4,5\text{-dinitrochrysazinate})_2DMF_4]$ forms red plate crystals and crystallises in the space group $P2_1/n$. The complex sits on an inversion centre so that the two nickel atoms are symmetrically equivalent. The Ni^{2+} ions and 4,5-dinitrochrysazinate dianions are coordinated in a dimeric motif like **CuChrys-1** and **CuChrys-2**, but with the 4,5-dinitrochrysazinate molecules tilted out of the plane of the Ni-O coordination. The chrysazin cores are bent and distorted out of planarity by the steric clash of the nitro groups in the 4 and 5 positions with the carbonyl in the 10 position. The DMF molecules coordinate above and below the plane of the dimeric unit, giving an octahedral coordination environment for each Ni^{2+}.

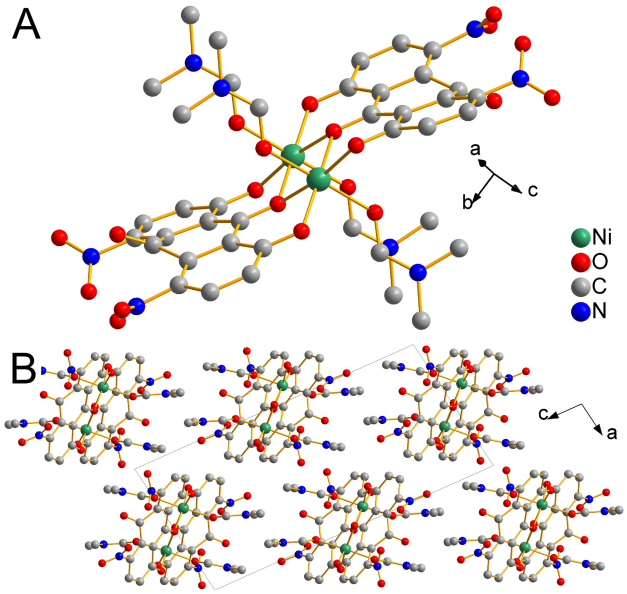

Fig. 11 Structure of $[Ni_2(4,5\text{-dinitrochrysazinate})_2DMF_4]$, **NiNOChrys-1**. (A) View of the complex. (B) Packing of the complex.

Concentration mmol/ml	Ligand:Metal stoichiometry					
	3:1	2:1	1:1	1:1.5	1:2	1:3
0.016	-	-	-	-	-	-
0.04	-	-	-	-	-	-
0.08	-	-	-	-	-	-
0.16	-	-	-	1	1	1

Table 2 Results of a high-throughput reaction between $Co(AcO)_2\cdot 4H_2O$ and chrysazin in DMF at 90 °C. The concentration given is [metal + ligand]. **1** = **CoChrys-1**, $[Co_{12}(Chrysazinate)_6(AcO)_{12}DMF_6]\cdot 6(DMF)$. Uncoloured cells correspond to reactions that left no crystalline solid.

High-throughput synthesis

To understand the synthetic trends in the chrysazin system, we carried out high-throughput screening reactions with acetates of manganese, iron, cobalt, nickel and copper. Mn and Fe gave no solid products; for Co, Ni and Cu, the results are summarised below.

Cobalt + chrysazin: effect of varying ligand:metal ratio and concentration CoChrys-1 forms only at the highest concentration studied and forms best at low ligand:metal ratios (Table 2). Large black single crystals of **CoChrys-1** were obtained at a ligand:metal ratio of 1:2 and a concentration of 0.16 mmol/ml; these crystals were of sufficient size and quality for the structures to be solved using single-crystal diffraction. The reaction was then scaled up using the method given in sec-

Concentration mmol/ml	Ligand:Metal stoichiometry					
	3:1	2:1	1:1	1:1.5	1:2	1:3
0.016	-	-	-	-	1	*a*
0.04	-	-	1	1	1	1 *b*
0.08	-	-	1	1 *c*	1 *c*	1
0.16	*d*	-	1	1	1	1

Table 3 Results of a high-throughput reaction between $Ni(AcO)_2{\cdot}4H_2O$ and chrysazin in DMF at 90 °C. The concentration given is [metal + ligand]. = **NiChrys-1**, $[Ni_{12}(Chrysazinate)_6(AcO)_{12}DMF_6]{\cdot}6(DMF)$. ***a*** - Only two peaks visible in the powder pattern, could be a new phase or possibly **NiChrys-1** with preferred orientation. ***b*** - Peak splitting at low angles, similar to **NiChrys-1** that has degraded over time. ***c*** - extra peak at $2\theta = 11.9°$, which is possibly due to the pure ligand. ***d*** - Unidentified phase. Uncoloured cells correspond to reactions that left no crystalline solid.

Concentration mmol/ml	Ligand:Metal stoichiometry					
	3:1	2:1	1:1	1:1.5	1:2	1:3
0.016	4	4	1 4	1 4	1 4 *a*	1
0.04	4	4	1 4	1 4 *a*	1 4 *a*	1
0.08	4	4	4	4	4	4
0.16	4	4	4	4	4	4

Table 4 Results of a high-throughput reaction between $Cu(AcO)_2.H_2O$ and chrysazin in DMF at 90 °C. The concentration given is [metal + ligand]. **1** = **CuChrys-1**, $[Cu_2(Chrysazinate)_2]$. **4** = **CuChrys-4**. ***a*** - These PXRD patterns also contained one or two peaks which could not be assigned.

tion S1.4. **CoChrys-2** and **CoChrys-3** form only with the use of different reagents (additional pyridine for **CoChrys-2** and $Co(OH)_2$ as Co source for **CoChrys-3**), and so it is unsurprising that they were not observed in this high-throughput study.

Nickel + chrysazin: effect of varying ligand:metal ratio and concentration Similarly to **CoChrys-1**, **NiChrys-1** forms best at low ligand:metal ratios; however, **NiChrys-1** forms over a wider range of concentrations than **CoChrys-1**. Increasing the concentration gives larger crystals and higher yields of **NiChrys-1**. **NiChrys-2** was not observed in the high-throughput investigation, despite its discovery in a larger scale reaction with the same composition and temperature. A number of the products showed PXRD peaks that could not be assigned to known phases. For ***a***-***c*** (Table 3), the small number of unidentified peaks and the uncertainty due to preferred orientation make it impossible to unambiguously identify the extra phases present. The preferred orientation could not be dealt with by griding the sample because the structure of **NiChrys-1** degrades upon grinding. For ***d*** (Table 3), only a small amount of powder was obtained and it has not been possible to grow single crystals for structural identification.

Copper + chrysazin: effect of varying ligand:metal ratio and concentration Like **CoChrys-1** and **NiChrys-1**, **CuChrys-1** was found to form best at low ligand:metal ratios; however, Cu gave higher yields and larger crystals at low concentrations, in contrast to Co and Ni. Pure product was obtained when using three equivalents of Cu(II) to each equivalent of ligand and concentrations of 0.04 mmol/ml and 0.016 mmol/ml (Table 4). If a high ligand:metal ratio, or high concentration, is used in the reaction between copper(II) and chrysazin, a red powder, **CuChrys-4** is formed. Unfortunately, it has not been possible to grow single crystals of this phase, and the PXRD pattern was not of sufficient quality for ab initio structure solution. This powder contains a crystalline phase which gives a reproducible PXRD pattern (Fig. S4), suggesting that the material is likely to be a single, new phase. Elemental analysis for this phase is consistent with a composition $Cu(HChrysazinate)_2$, where each chrysazin is singly deprotonated (Calculated mass %: C 62.05; H 2.60; N 0.00; Cu 11.73; O 233.62. Found mass %: C 61.86; H 2.85; N 0.47). The IR spectrum of **CuChrys-4** contains a broad peak at 3120 cm^{-1}, which would match to the remaining protonated hydroxl group on chrysazin (Fig. S2); such a peak is absent in the IR spectrum of **CuChrys-1**. The assignment of the composition is further reinforced by the observation that upon treatment with a flow of 5% H_2 in N_2 gas at 150 °C, **CuChrys-1** reacts to form **CuChrys-4** and elemental copper (Fig. S5).

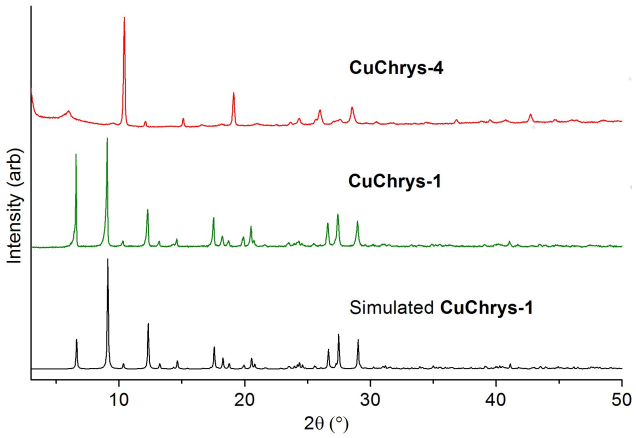

Fig. 12 PXRD patterns of the unidentified phase **CuChrys-4** in comparison to the experimental and simulated diffraction patterns of **CuChrys-1**.

Synthetic trends

In the Cu system, low metal:ligand ratios favour **CuChrys-1**, as expected from the stoichiometries of the products. The fact that **CuChrys-1** forms preferentially at low reagent concentrations suggests that the products are in a reversible set of reactions with the unbound reagents and that **CuChrys-4** is a kinetic product and **CuChrys-1** is a thermodynamic product. At high reagent concentrations, **CuChrys-4** rapidly forms and precipitates; at lower reagent concentrations, **CuChrys-4** only reaches a lower concentration, so does not precipitate to the same degree and **CuChrys-1** has more time to form. An alternative explanation would be that by changing the concentration of reagents, we alter other factors such as the pH of the solution and that this directs the product selectivity. To differentiate between these hypotheses, we reacted chrysazin (0.008 mmol) with $Cu(AcO)_2$ (0.016 mmol) in DMF over a range of different times (1, 3, 18 and 48 hours - see ESI for full synthetic procedure). It was confirmed that **CuChrys-4** forms early on in the reaction and disappears over the course of the reaction (Fig. S2.4). A new phase, **CuChrys-2**, was discovered in this experiment and structurally characterised by SCXRD. **CuChrys-2** forms alongside **CuChrys-1** and **CuChrys-4**, but disappears from the reaction over time, leaving **CuChrys-1**. As a result, it has not been possible to isolate a pure phase of **CuChrys-2**.

Ni and Co both form twelve-membered ring complexes (**NiChrys-1** and **CoChrys-1**), as well as smaller complexes (**NiChrys-2**, with six nickel atoms, and **CoChrys-2**, with three cobalt atoms). The similarity of the smaller complexes to the motif that makes up the twelve-membered rings, suggests that there is an equilibrium in solution between the twelve-membered complexes and smaller building units. **NiChrys-1** and **CoChrys-1** are, however, the dominant products. In the Ni system, **NiChrys-2** has only been identified as a minor phase, next to the doiminant **NiChrys-1**. In the cobalt system, **CoChrys-2** forms only with the addition of pyridine to the reaction, while **CoChrys-3** requires the use of $Co(OH)_2$ as a reactant.

Electronic structure of CuChrys-1

The metallic appearance and short plane-plane π-stacking distance in **CuChrys-1** led us to investigate the electronic properties of **CuChrys-1**, with a view to exploring its use as an organic-inorganic hybrid semiconductor. We carried out single-crystal conductivity measurements using our recently reported microelectrode setup[31] and powder conductivity measurements on pressed powder pellets,[32] and found that the as-synthesised samples of **CuChrys-1** were insulating. To understand this observation, we carried out plane-wave pseudopotential DFT[33–35] calculations as implemented in the CASTEP[36] and OPTADOS[37] packages (full details are given in the ESI).

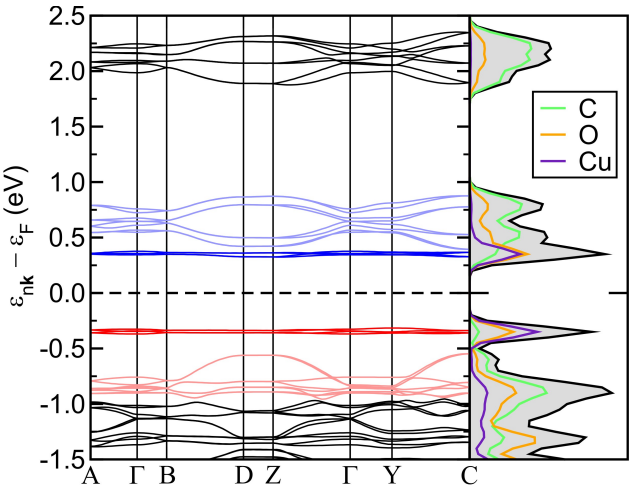

Fig. 13 Band structure and partial density of states for **CuChrys-1** calculated using DFT, with a Gaussian smearing applied to the energies. Hydrogen is not shown as it has no significant electron density in this energy range. The HOMO levels arising from the Cu $d_{x^2-y^2}$ /O sp^2 orbitals are shown in dark red. The more disperse filled bands due to the overlap of π orbitals on chrysazinate are shown in pale red. The LUMO levels (Cu $d_{x^2-y^2}$ /O sp^2) are shown in dark blue. The disperse unfilled bands (overlapped π orbitals on chrysazinate) are shown in pale blue.

Our calculations showed that there are disperse bands due to the overlap of the π/π^* orbitals centred at 0.49 eV above and 0.67 eV below the Fermi energy; however, these are not the frontier molecular orbitals (Fig. 13). There are flat bands (localised orbitals) at 0.35 eV above and 0.345 eV below the Fermi energy. These "bands" can be identified from the electron density plots as the orbitals arising from the interaction of the Cu $d_{x^2-y^2}$ orbitals with the O sp^2 orbitals, as expected for a Cu^{2+} ion (d^9 electronic configuration) in a square planar (or Jahn-Teller distorted octahedral) environment. These localised orbitals, although symmetrically orthogonal to the disperse π-bands, will act as charge traps and therefore prevent the disperse bands from obtaining the partial occupation necessary for electronic conductivity. We investigated computationally whether applied pressure might lead to a transition to a conducting state (Fig. S2.6). Calculations done at increased pressure (5 GPa and 10 GPa) show an increased dispersion of the π/π^* bands, as expected from the better overlap of the orbitals; however, even these large pressures are insufficient to cause an overlap in the energies of the π/π^* band and the HOMO/LUMO.

Conclusions

We have synthesised a diverse set of coordination complexes, with up to 12 metal atoms per complex, in which the ligand chrysazinate adopts a range of binding modes including chelating and bridging modes. The synthetic chemistry of these compounds was investigated using high-throughput synthesis, which enabled us to discover a new compound, optimise synthetic conditions and showed that the reaction of Cu and chrysazin is a dynamic equilibrium with multiple products. One of these products, **CuChrys-1**, showed a remarkably short (<3.26 Å) π-π distance, which led us to study the electronic properties of this material. **CuChrys-1** was found to be insulating using single-crystal and powder measurements. This can be explained by our DFT calculations: in spite of the presence of well-dispersed π/π^* bands, the frontier orbitals are localised orbitals centred on Cu, so oxidation/reduction of the complex would not lead to partial occupancy of the disperse bands.

Acknowledgements

PJB acknowledges an EPSRC Doctoral Prize fellowship. BM acknowledges an EPSRC PhD studentship. SH thanks the Alexander von Humboldt Foundation for a Feodor Lynen Fellowship. This work was supported by an Advanced Investigator Award to AKC from the European Research Council (ERC) and by the World Premier International Research Center Initiative on "Materials Nanoarchitectonics (WPI-MANA)" from MEXT, Japan. We thank the EPSRC UK National Crystallography Service at the University of Southampton for the collection of crystallographic data, including work at Diamond Light Source (beamtime award MT8521 on I19).

References

1 A. Navas Diaz, *J. Photochem. Photobiol., A*, 1990, **53**, 141–167.
2 M. Mamada, D. Kumaki, J.-I. Nishida, S. Tokito and Y. Yamashita, *ACS Appl. Mater. Interfaces*, 2010, **2**, 1303–7.
3 F. Gándara, N. Snejko, A. D. Andrés, J. R. Fernandez, J. C. Gómez-Sal, E. Gutierrez-Puebla and A. Monge, *RSC Adv.*, 2012, **2**, 949.
4 C. Dimitrakopoulos and P. Malenfant, *Adv. Mater.*, 2002, **14**, 99–117.
5 G. R. Hutchison, M. A. Ratner and T. J. Marks, *J. Am. Chem. Soc.*, 2005, **127**, 16866–81.
6 Y. Geng, H.-B. Li, S.-X. Wu and Z.-M. Su, *J. Mater. Chem.*, 2012, **22**, 20840.
7 S. Pola, C.-T. Kuo, W.-T. Peng, M. M. Islam, I. Chao and Y.-T. Tao, *Chem. Mater.*, 2012, **24**, 2566–2571.
8 A. N. Sokolov, T. Friščić and L. R. MacGillivray, *J. Am. Chem. Soc.*, 2006, **128**, 2806–7.
9 J. D. Furman, R. P. Burwood, M. Tang, A. A. Mikhailovsky and A. K. Cheetham, *J. Mater. Chem.*, 2011, **21**, 6595.
10 E. E. Langdon-Jones and S. J. Pope, *Coord. Chem. Rev.*, 2014, **269**, 32–53.
11 M. Kadarkaraisamy and A. G. Sykes, *Inorg. Chem.*, 2006, **45**, 779–86.
12 M. Kadarkaraisamy and A. G. Sykes, *Polyhedron*, 2007, **26**, 1323–1330.
13 K. Mariappan and P. N. Basa, *Inorg. Chim. Acta*, 2011, **366**, 344–349.
14 V. Y. Fain, B. E. Zaitsev and M. A. Ryabov, *Russ. J. Coord. Chem.*, 2004, **30**, 360–364.
15 A. L. Rohl, M. Moret, W. Kaminsky, K. Claborn, J. J. McKinnon and B. Kahr, *Cryst. Growth Des.*, 2008, **8**, 4517–4525.
16 N. Stock, *Microporous and Mesoporous Materials*, 2010, **129**, 287–295.
17 N. Stock and S. Biswas, *Chemical reviews*, 2012, **112**, 933–69.
18 O. V. Dolomanov, L. J. Bourhis, R. J. Gildea, J. A. K. Howard and H. Puschmann, *J. Appl. Crystallogr.*, 2009, **42**, 339–341.
19 J. Szejtli, *Chem. Rev.*, 1998, **98**, 1743–1754.
20 J. W. Lee, S. Samal, N. Selvapalam, H.-J. Kim and K. Kim, *Acc. Chem. Res.*, 2003, **36**, 621–30.
21 A. L. Spek, *Acta Crystallographica Section C Structural Chemistry*, 2015, **71**, 9–18.
22 P. van der Sluis and A. L. Spek, *Acta Crystallogr., Sect. A: Found. Crystallogr.*, 1990, **46**, 194–201.
23 J. Huheey, E. Keiter, R. Keiter and O. Medhi, *Inorganic Chemistry: Principles of Structure and Reactivity*, Pearson Education, 2006.
24 R. D. Shannon and C. T. Prewitt, *Acta Crystallogr., Sect. B: Struct. Sci., Cryst. Eng. Mater.*, 1969, **25**, 925–946.
25 R. D. Shannon, *Acta Crystallogr., Sect. A: Found. Crystallogr.*, 1976, **32**, 751–767.
26 N. Greenwood and A. Earnshaw, *Chemistry of the Elements*, Elsevier Science, 1997.
27 V. Sicilia, J. Forniés, J. M. Casas, A. Martín, J. A. López, C. Larraz, P. Borja, C. Ovejero, D. Tordera and H. Bolink, *Inorganic Chemistry*, 2012, **51**, 3427–3435.
28 Y. Chen, J. Dou, D. Li and S. Wang, *Inorganic Chemistry Communications*, 2010, **13**, 167–170.
29 C. Janiak, *J. Chem. Soc., Dalton Trans.*, 2000, 3885–3896.
30 R. A. Heintz, H. Zhao, X. Ouyang, G. Grandinetti, J. Cowen and K. R. Dunbar, *Inorganic Chemistry*, 1999, **38**, 144–156.
31 S. Tominaka, S. Henke and A. K. Cheetham, *CrystEngComm*, 2013, **15**, 9400.
32 P. J. Beldon, S. Tominaka, P. Singh, T. Saha Dasgupta, E. G. Bithell and A. K. Cheetham, *Chem. Commun.*, 2014, **50**, 3955–7.
33 P. Hohenberg and W. Kohn, *Phys. Rev.*, 1964, **136**, B864–B871.
34 W. Kohn and L. J. Sham, *Phys. Rev.*, 1965, **140**, A1133–A1138.
35 M. C. Payne, M. P. Teter, D. C. Allan, T. A. Arias and J. D. Joannopoulos, *Rev. Mod. Phys.*, 1992, **64**, 1045–1097.
36 S. J. Clark, M. D. Segall, C. J. Pickard, P. J. Hasnip, M. I. J. Probert, K. Refson and M. C. Payne, *Z. Kristallogr.*, 2005, **220**, 567.
37 A. J. Morris, R. J. Nicholls, C. J. Pickard and J. R. Yates, *Comp. Phys. Comm.*, 2014, **185**, 1477 – 1485.